Neurotherapeutics 21 (2024) e00367

Contents lists available at ScienceDirect

Neurotherapeutics

journal homepage: www.sciencedirect.com/journal/neurotherapeutics

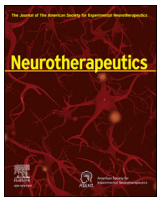

Original Article

Structural network topologies are associated with deep brain stimulation outcomes in Meige syndrome

Bin Liu [a,b,1], Zhiqi Mao [b,1], Xinyuan Yan [c], Hang Yang [d], Junpeng Xu [a,b], Zhebin Feng [a,b], Yanyang Zhang [b,*], Xinguang Yu [b,*]

[a] Medical School of Chinese PLA, Beijing, 100853, China
[b] Department of Neurosurgery, The First Medical Center of Chinese PLA General Hospital, Beijing, 100853, China
[c] Department of Psychiatry, University of Minnesota Medical School, Minneapolis, MN, USA
[d] Chinese Institute for Brain Research, Beijing, 102206, China

ARTICLE INFO

Keywords:
Meige syndrome
Structural covariance network
Graph theory
Deep brain stimulation
Clinical outcome

ABSTRACT

Deep brain stimulation (DBS) is an effective therapy for Meige syndrome (MS). However, the DBS efficacy varies across MS patients and the factors contributing to the variable responses remain enigmatic. We aim to explain the difference in DBS efficacy from a network perspective. We collected preoperative T1-weighted MRI images of 76 MS patients who received DBS in our center. According to the symptomatic improvement rates, all MS patients were divided into two groups: the high improvement group (HIG) and the low improvement group (LIG). We constructed group-level structural covariance networks in each group and compared the graph-based topological properties and interregional connections between groups. Subsequent functional annotation and correlation analyses were also conducted. The results indicated that HIG showed a higher clustering coefficient, longer characteristic path length, lower small-world index, and lower global efficiency compared with LIG. Different nodal betweennesses and degrees between groups were mainly identified in the precuneus, sensorimotor cortex, and subcortical nuclei, among which the gray matter volume of the left precentral gyrus and left thalamus were positively correlated with the symptomatic improvement rates. Moreover, HIG had enhanced interregional connections within the somatomotor network and between the somatomotor network and default-mode network relative to LIG. We concluded that the high and low DBS responders have notable differences in large-scale network architectures. Our study sheds light on the structural network underpinnings of varying DBS responses in MS patients.

Introduction

Meige syndrome (MS) is a subtype of segmental dystonia, initially manifesting as blepharospasm and subsequently involving oromandibular and cervical muscles progressively [1]. The low incidence and the absence of megascopic brain lesions on routine MRI images impede the disclosure of the underlying neurobiological mechanisms.

Deep brain stimulation (DBS) has emerged as a recognized, secure, and effective therapeutic approach for MS, even in cases resistant to botulinum toxin injections [1,2]. The globus pallidus internus (GPi) was once regarded as the preferred DBS target for MS [3,4]. However, recent accumulating evidence suggests that stimulating the subthalamic nucleus (STN) can yield comparable outcomes [5–7]. Considering the advantages of faster therapeutic response and lower energy consumption, we prefer to target STN instead of GPi for MS patients in our center. However, the challenge is that no matter which target to be stimulated, some MS patients have good treatment effects, while others do not. And we know little about what drives the individual differences.

To address this issue, previous clinical studies have sought potential clinical predictors of DBS prognosis, including disease duration, patient age at the time of surgery, the choice of stimulation targets, and follow-up duration [8–10]. In addition, several neuroimaging investigations have attempted to identify specific brain regions linked to DBS outcomes, such as the precentral gyrus, the supplementary motor area, and the cerebellum [11–14]. However, these efforts have yielded unstable and inconsistent predictive power. We hypothesized that this puzzle may

* Corresponding authors.
E-mail addresses: sjwkzyy@163.com (Y. Zhang), yuxinguang_301@163.com (X. Yu).
[1] These authors have contributed equally to this work.

https://doi.org/10.1016/j.neurot.2024.e00367
Received 4 November 2023; Received in revised form 18 April 2024; Accepted 19 April 2024

need evidence from the network instead of the single brain region. Because MS is precisely considered a brain network disorder, which is supported by an increasing body of modern neuroimaging studies uncovering structural and functional abnormalities in multiple regions and widespread disturbance of their connectivity [15–19]. Unfortunately, no study has explained the difference in STN-DBS efficacy from a network perspective so far.

Structural covariance networks (SCNs), constructed at the group level, elucidate the coordinated changes in gray matter (GM) volume or thickness among different regions of the brain [20,21]. It is assumed to reflect anatomical connectivity, mutually trophic effects of synapses, and common experience-driven plasticity [22]. SCN is replicable and heritable in both healthy individuals and patients, and can track disease-related topological changes [22]. GM morphology covariance patterns have been associated with functional coactivation [23,24], diffusional connectivity [25,26], and gene expression [27]. Moreover, functional abnormalities tend to be interpreted by corresponding structural changes [28]. Notably, unlike DBS for Parkinson's disease, which often produces immediate effects, DBS for dystonia, despite targeting the same area, may require several weeks or even months to demonstrate efficacy [8]. This suggests that DBS may not directly alter the functional network but may instead fundamentally reshape the structural architecture. Therefore, all the above evidence indicates that investigating the fine-grained differences in SCN architectures between good and poor DBS responders is urgent and essential.

Graph theory analysis provides a robust framework for investigating brain circuit reorganization by quantifying the topological properties of brain networks [29]. While graph-based SCN measures have been explored in the context of focal dystonia in comparison to neurotypical individuals [16], no study has correlated these measures with STN-DBS outcomes in MS patients.

Here, we constructed the volume-based, cortex-wide SCNs in two groups separately: those who show substantial improvement (the high improvement group, HIG) and those who show limited improvement (the low improvement group, LIG). Next, we compared the topological patterns and interregional connections between the two groups. For those brain regions showing discrepant nodal centralities, we annotated their cognitive functions and correlated them with the symptomatic improvement rates. Our aim is to identify structural fingerprints linked to STN-DBS outcomes.

Methods

Participants

We retrospectively collected clinical information of all MS patients who underwent STN-DBS surgery at the Chinese People's Liberation Army General Hospital from October 2015 to May 2023. Inclusion criteria: (i) idiopathic MS diagnosed by experienced neurologists; (ii) over a three-month interval between scanning and the last botulinum toxin injection (if any). Exclusion criteria: (i) secondary MS or dystonia involving other body sites; (ii) longtime (>1 year) exposure to neuropsychiatric drugs before MS onset; (iii) combined with other neurological diseases, such as symptomatic stroke, Parkinson's disease, essential tremor, epilepsy, and Alzheimer's disease; (vi) encountering surgery-related adverse effects; (v) low-quality MRI images. To keep group homogeneity, we only included MS patients treated by STN-DBS (eight GPi-DBS cases were excluded). The exact neurosurgical procedure has been described previously [6]. All patients were scheduled for an intraoperative MRI or a postoperative CT to ensure the accurate implantation of DBS electrodes. To control the potential influence of electrode position on DBS efficacy, we also excluded those poorly responsive patients whose postoperative imaging fusion revealed an over 3 mm displacement of either electrode tip from the predefined target (two patients were excluded).

Symptomatic severity was quantified preoperatively (around the time of MRI scanning) and postoperatively (at least three months after DBS activation) with the Burke-Fahn-Marsden Dystonia Rating Scale movement subscale (BFMDRS-M), which is the most popular scale to quantify the symptomatic severity for MS patients [30]. We sorted all MS patients according to the improvement rates of BFMDRS-M and dichotomized them into the high-improvement group (HIG, n = 38) and the low-improvement group (LIG, n = 38) from the median point. All the demographic and clinical information is presented in Table 1.

This study was approved by the local ethical committee of the Chinese PLA General Hospital and carried out in accordance with the Declaration of Helsinki. Written informed consent was obtained from all participants.

MRI data acquisition

All images (three-dimensional T1 weighted structural image) were acquired using a 3 T MR system (Discovery MR750, General Electric) with a sagittal fast spoiled gradient-echo sequence (TR: 6.7 ms, TE: 2.9 ms, flip angle: 7°, FOV: 256 × 256 mm^2, number of slices: 192, slice thickness: 1 mm with no gap) one week before DBS surgery.

Data preprocessing and quality control

All images were inspected visually. Scans with evident head motion artifacts or poor gray/white matter differentiation were excluded (one patient). The T1-weighted structural images were processed and analyzed in the Statistical Parametric Mapping (SPM12) software (http://www.fil.ion.ucl.ac.uk/spm), which was implemented in the Matlab (R2022b) environment (https://www.mathworks.com/). Images were segmented into GM, white matter, and cerebrospinal fluid, spatially

Table 1
Between-group comparison of clinical information.

	HIG (n = 38)	LIG (n = 38)	X^2/T/Z value	*P* value
Sex (male/female)	17/21	11/27	2.036[c]	0.154[c]
Age (mean ± SD)	55.89 ± 9.97	58.08 ± 8.25	−1.04[a]	0.302[a]
Education (year)	8.79 ± 4.25	8.95 ± 3.37	−0.179[a]	0.962[a]
Handedness(R/L)	37/1	36/2	0.347[c]	0.556[c]
Disease duration (year)	4.23 ± 4.77	4.57 ± 4.46	−1.224[b]	0.221[b]
Botulinum injection (times)	1.24 ± 1.46	1.34 ± 1.81	−0.131[b]	0.896[b]
Pre-BFMDRS-M	11.45 ± 5.08	12.84 ± 5.54	−1.408[b]	0.159[b]
Post-BFMDRS-M	2.58 ± 2.31	8.47 ± 4.34	**−6.258**[b]	**< 0.001**[b]
BFMDRS-M improvement (%)	85.53 ± 10.71	33.81 ± 15.86	**−7.507**[b]	**< 0.001**[b]
Follow-up time (months)	8.66 ± 2.85	8.20 ± 3.39	0.575[b]	0.575[b]

Data is presented as mean ± standard deviation. HIG, high improvement group; LIG, low improvement group. BFMDRS-M, Burke-Fahn-Marsden Dystonia Rating Scale movement subscale.

[a] two-sample *t*-test.

[b] Mann-Whitney *U* test.

[c] chi-square test.

normalized to the standard Montreal Neurological Institute (MNI) space, and further modulated to preserve tissue volume by using the default parameters of the *Segment* module in the Computational Anatomy Toolbox (CAT12, http://www.neuro.uni-jena.de/cat). Subsequently, the resultant images were checked for homogeneity using the *Data Quality* module in CAT12. Flagged images (i.e., the mean absolute Z score >1.0) were visually inspected before being discarded (two patients). Finally, all images were smoothed with an 8 mm full-width at half-maximum Gaussian kernel.

Construction of structural covariance networks

We parcellated the segmented, normalized and smoothed GM images into 120 regions of interest (ROIs) defined by the automated anatomical labeling 2 (AAL2) atlas, which is an upgraded version of the AAL atlas (the most commonly used volume parcellation schemes) with further parcellation of the orbitofrontal gyrus [31]. The mean GM volume of each ROI was extracted and regressed out the effects of age, sex, total intracranial volume (TIV), and education. Since both the cerebrum and cerebellum have their network organizations [32,33], here to keep consistent with other analogous studies, we focused only on the cerebral cortex (94 ROIs) and ignored the cerebellar ROIs. Pairwise Pearson correlations between ROIs across subjects were calculated for HIG and LIG separately, yielding a 94 × 94 group-level association matrix in each group (Fig. S2), with each value in the matrix representing the co-varied strength (Pearson correlation coefficient) of GM volume between any two brain regions (Fig. 1).

Given there existed no conclusive approaches for selecting a single network density, we set a range of sparsity ([0.05–0.35], with interval steps of 0.01) to produce a series of binary undirected networks in each group. The lower limit was defined by the log(N)/(N-1) formula (N = ROI numbers), while the upper limit was set to keep the small-world index larger than 1.1 for all patients [34]. Each sparsity corresponded to a threshold, and only connections above the threshold were preserved and set to 1, while other connections were set to 0. This density range enabled between-group comparisons of each topological metric with a comparable number of edges, but without bringing in disconnections or losing small-world properties [35,36]. To generate a summary metric, we plotted curves showing how the measures of interest change as a function of sparsity, and we computed the area under the curve (AUC) for each network attribute.

Graph theory analyses

For each network at each sparsity threshold, we calculated global and nodal network measures. First, the segregation (clustering coefficient, C_p, and local efficiency, E_{local}) and integration (characteristic path length, L_p, and global efficiency, E_{global}) properties of structural networks were computed using the Brain Connectivity Toolbox implemented in Matlab [37]. To calculate the small-world index (Sigma), we generated 100 random networks that had the same degree distributions as the real networks, and then C_p and L_p were normalized by the corresponding measures averaged by the 100 random networks. Second, two nodal centrality metrics (betweenness and degree) were

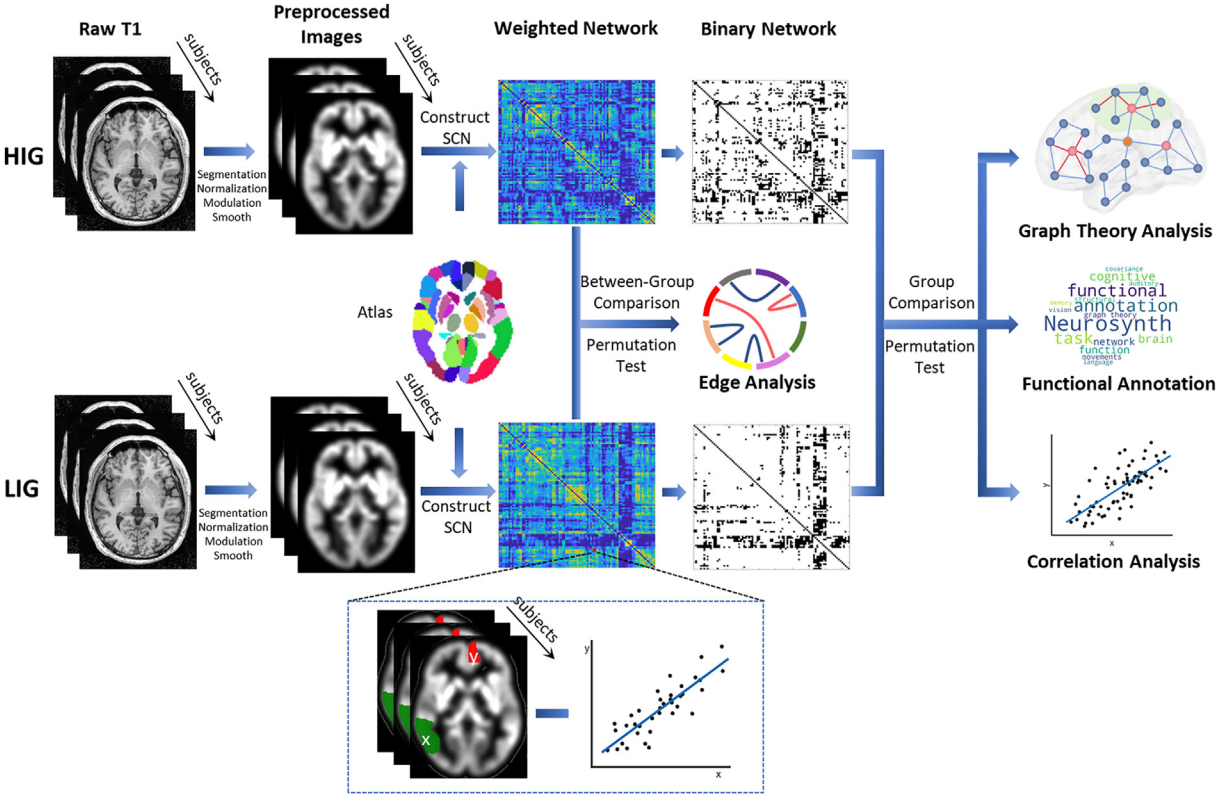

Fig. 1. Flowchart of SCN construction and subsequent analyses. From left to right: in each group, T1-weighted images were preprocessed before being parcellated into ROIs according to the selected atlas. The mean GM volume of each ROI was extracted to calculate the pairwise Pearson correlation coefficients, thereby constructing two group-level association matrices (i.e., SCNs). Between-group comparison of interregional connectivity was conducted through non-parametric permutation tests. Subsequently, a range of sparsity was set to threshold the SCNs into a series of binary undirected networks, based on which graph theory analyses were conducted. For those brain regions showing discrepant nodal centralities, functional annotation and correlation analyses were further explored. HIG, high improvement group; LIG, low improvement group; SCN, structural covariance network; ROI, region of interest.

calculated for each anatomical ROI at each sparsity threshold. Finally, we compared and visualized the above global and nodal topological properties between HIG and LIG. Detailed interpretations of these graph theory metrics are summarized in the Supplementary Material.

Functional annotation of differential nodes

The brain regions showing significant differences in nodal centralities were annotated functionally by using the *Decoder* module on the Neurosynth platform (https://neurosynth.org/decode) [38], which includes over 1300 meta-analytic brain maps synthesized from over 14,300 functional MRI studies, with each map corresponding to a cognitive term. Specifically, the significant nodes were extracted from the selected atlas and integrated into a binary mask by using the *Image Calculator* module in SPM12. After submitting the mask to the Neurosynth database, we would obtain hundreds of cognitive terms, which reflect the functions of these brain regions. The resultant terms were filtered (correlation >0.1) and visualized on a word-cloud plot after removing those anatomical (e.g. 'motor cortex', 'parietal') and non-specific terms (e.g. 'primary', 'tasks'). In this part, to show the functional differences more comprehensively, we included all brain regions showing different betweennesses or degrees (as per $P < 0.05$, uncorrected).

Correlation analyses of differential nodes

For those regions showing significant differences in nodal centralities, we extracted their mean GM volume in each subject and controlled the effects of age, sex, TIV, and education by linear regression. The standardized residuals were used to test their linear correlation with the BFMDRS-M improvement rates for all MS patients. In this part, to limit the number of comparisons, we only investigated those brain regions showing significant differences in both betweenness and degree (as per $P < 0.05$, uncorrected).

Interregional connectivity analyses

We further identify the between-group differences in the interregional correlations of both group-level weighted SCNs, aiming to localize the region pairs related to STN-DBS efficacy. Moreover, to define which priori network module the discrepant edges belong to, we mapped each atlas ROI to the seven large-scale functional networks proposed by Thomas Yeo [32], with the largest voxel-wise overlapping as the final match [39]. Subcortical nodes were defined as an eighth subcortical network.

Validation

To validate the findings of network analyses, we repeated the procedures by using another structural atlas (Harvard-Oxford Atlas, HOA) [40], which produced two 110 × 110 correlation matrices at the group level after omitting the cerebellum, brain stem, and ventricles. The graph-based topological properties and the interregional correlations were explored and compared between groups using the same thresholding and statistical methods.

Statistical analyses

Clinical and demographic variables were compared using two-sample t-tests (normal distribution) or the Mann-Whitney *U* test (non-normal distribution) for continuous variables and the chi-square test for categorical variables in SPSS 26 (IBM, Armonk, NY). The significance level was set at $P < 0.05$ (two-tailed).

For network graph theory analysis, we conducted non-parametric permutation tests (10,000 replications) to investigate whether the differences in network parameters between HIG and LIG were induced by chance, by randomly reassigning the group labels while keeping the same number of cases within each group. We calculated the distribution of the 10,000 between-group AUC differences in each graph parameter and observed whether the real between-group difference was localized within the 95% confidence interval of this distribution. For global and nodal network metrics, the significant level was set at $P < 0.05$ (Benjamini-Hochberg FDR-corrected, two-tailed). Likewise, permutation tests were used to detect significantly altered edges in the interregional connectivity analysis ($P < 0.001$, uncorrected, two-tailed).

For correlation analyses, Spearman correlation coefficients were used owing to the non-normal distribution of BFMDRS-M improvement rates, with significance levels set at $P < 0.0125$ (for AAL2) and $P < 0.01$ (for HOA), Bonferroni corrected for multiple comparisons (0.05/the number of tested brain regions).

Results

Clinical and demographic information

After quality control, a total of 76 MS patients (n = 38 for each group) were included (Table 1). HIG showed higher postoperative BFMDRS-M scores and BFMDRS-M improvement rates compared to LIG ($P < 0.001$). No significant between-group differences were detected in sex, age, education level, disease duration, times of botulinum injection, preoperative BFMDRS-M scores, and follow-up time (all $P > 0.05$). The stimulation parameters and coordinates of activated contacts in the standard space were provided in Table S4 and Table S5, respectively.

Between-group differences in global and nodal graph-based network measures

The SCNs constructed in both groups showed small-world organizations across the selected sparsity range (Fig. 2A). As for global network measures (Fig. 2B), HIG presented significantly higher AUC values of C_p ($P = 0.012$, FDR-corrected) and L_p ($P = 0.012$, FDR-corrected) across the sparsity compared to LIG, evidencing a more regular network architecture (Fig. S1). Accordingly, the Sigma of HIG was significantly lower than that of LIG ($P = 0.035$, FDR-corrected). Furthermore, the comparisons of network efficiency revealed a significantly decreased E_{global} ($P = 0.012$, FDR-corrected) but undifferentiated E_{local} ($P = 0.891$, FDR-corrected). See Fig. S3 for detailed results for each measure at each network density.

As for nodal network measures, to show more potentially different brain regions, we listed and visualized all the results thresholded at $P < 0.05$ (uncorrected) (Fig. 3A, Table 2). Compared with LIG, HIG displayed increased nodal betweennesses in the left precentral gyrus, left supplementary motor area, right posterior cingulate gyrus, left postcentral gyrus, right postcentral gyrus, right inferior parietal gyrus, and right precuneus, but decreased nodal betweennesses in the left superior parietal gyrus, left thalamus, and left inferior temporal gyrus (all $P < 0.05$, uncorrected). Only the right precuneus survived correction for multiple comparisons ($P = 0.038$, FDR-corrected). Moreover, increased nodal degrees were observed in the left precentral gyrus, right calcarine fissure, and right precuneus, and reduced nodal degrees were detected in the right superior occipital gyrus, left putamen, right pallidum, left thalamus, and left inferior temporal gyrus (all $P < 0.05$, uncorrected). Only the left precentral gyrus ($P = 0.042$, FDR-corrected) and the right precuneus ($P = 0.019$, FDR-corrected) survived correction for multiple comparisons. Of note, four regions (i.e., right precuneus, left precentral gyrus, left thalamus, and left inferior temporal gyrus) displayed consistent alterations in both centrality measures, implying their robust correlations with STN-DBS outcomes. See Fig. S4 for detailed information about the between-group comparison of each region.

Functional annotation: nodes showing differences in nodal centralities

Functional annotation via the Neurosynth platform suggested that the nodes showing different betweennesses or degrees between groups

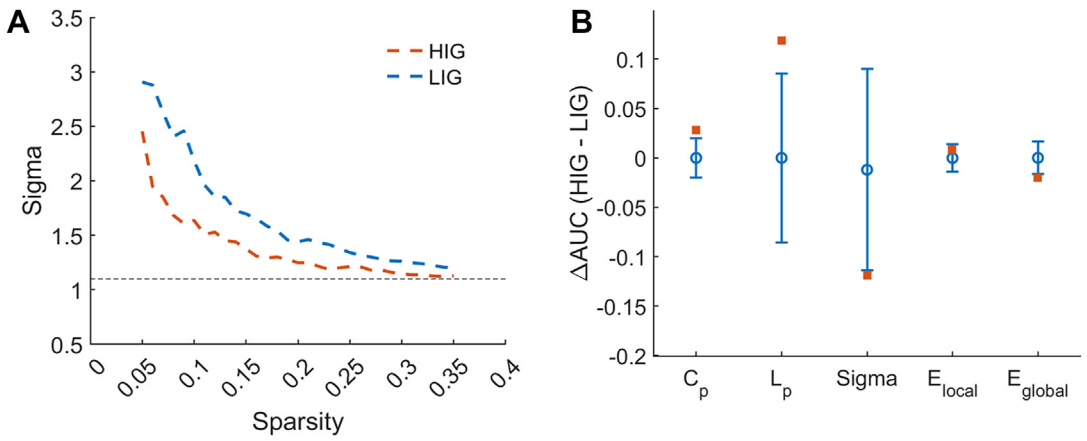

Fig. 2. Results of global network analyses. (A) Changes in small-world indices of the SCNs as a function of selected sparsity [0.05–0.35]. Both HIG (red line) and LIG (blue line) represent stable small-world attributes. The horizontal black dashed line indicates the defined criteria of a small-world network (Sigma ≥1.1). (B) Between-group differences in areas under the curve (AUC) values of global topological properties (clustering coefficient, C_p; characteristic path length, L_p; small-world attributes, Sigma; local efficiency, E_{local}; global efficiency, E_{global}). The red squares represent the real AUC differences between HIG and LIG. The blue lines denote the mean values (open circles) and the 95% confidence intervals of between-group AUC differences calculated from 10,000 permutation tests. A significant result is defined when the red square is located outside of the blue line ($P < 0.05$, two-tailed).

($P < 0.05$, uncorrected) were predominantly involved in the preparation, execution, and coordination of movements (Fig. 3B).

Clinical correlation analyses: nodes showing differences in nodal centralities

As shown in Fig. 3C, the BFMDRS-M improvement rates were positively correlated with the mean GM volume of the left precentral gyrus (r = 0.331, $P = 0.003$, Bonferroni corrected) and the left thalamus (r = 0.293, $P = 0.010$, Bonferroni corrected). Moreover, the GM volume of the right precuneus (r = 0.308, $P = 0.026$), albeit not surviving correction for multiple comparisons, showed a potential correlation with the BFMDRS-M improvement rates. No significant correlation was identified when the left inferior temporal gyrus (r = −0.182, $P = 0.116$) was tested.

Between-group differences in interregional connectivity

Compared with LIG, HIG showed more enhanced interregional connections, most of which were intra-network connections in the somatomotor network and inter-network links between the somatomotor network and the default-mode network (DMN) (Fig. 4, Table S6). The right postcentral gyrus, right precuneus, and left precentral gyrus contributed the most (involved in ≥ three differential edges). Furthermore, only one decreased connection (between the left angular gyrus and the right superior occipital gyrus) was detected.

Results of validation based on Harvard-Oxford Atlas

The network measures based on HOA parcellation showed similar results. Specifically, the SCNs constructed in both groups presented a stable small-world attribute (Fig. S5A), and the comparisons in global network metrics revealed significantly increased C_p ($P = 0.04$, FDR-corrected) and L_p ($P = 0.04$, FDR-corrected) but decreased Sigma ($P = 0.005$, FDR-corrected) and indifferent network efficiencies in HIG compared to LIG (Fig. S5B). Moreover, significant differences in both nodal centralities between groups were consistently found in the left precentral gyrus, right postcentral gyrus, right precuneus, posterior division of left superior temporal gyrus, and left thalamus (Fig. S6A, Table S1), among which the right precuneus ($P = 0.044$, FDR-corrected) survived correction for multiple comparisons. These regions were mainly associated with movement tasks and memory retrieval through Neurosynth annotation (Fig. S6B). For correlation analyses, the BFMDRS-M improvement rates were positively correlated with the mean GM volume of the left precentral gyrus (r = 0.293, $P = 0.009$, Bonferroni corrected) (Fig. S6C). For the comparisons of interregional connections, most of the enhanced edges were still within somatomotor network or between somatomotor network and DMN (Fig. S7), and the right postcentral gyrus, bilateral precuneus, and left precentral gyrus contributed the most (involved in ≥ three differential edges).

Discussion

Using SCNs and graph theory, we investigated the differences between HIG and LIG in global topological patterns, which revealed distinct information integration and segregation between groups. The discrepancies were mainly ascribed to the changes in interregional connectivity within somatomotor network or between somatomotor network and DMN. Further nodal topological comparisons, functional annotation, and correlation analyses together suggested that STN-DBS outcomes of MS were mainly associated with the changes in the precuneus, sensorimotor cortex, and subcortical nuclei. In this study, we only used the cortex and subcortical nuclei to construct the SCNs in both groups because most previous SCN studies have excluded the cerebellum. Moreover, both the resting-state functional MRI studies [33] and the task-related functional MRI studies [41,42] have demonstrated that the cerebrum and cerebellum have their own network organization framework, though they are connected structurally and functionally. Thus, it is reasonable to separate them for analysis. To the best of our knowledge, this is the first study to investigate the relationship between structural network integrity and STN-DBS efficacy.

Interpretation of the differences in global network measures

The constructed SCNs in both groups held a stable small-world organization throughout the sparsity range, which suggested that the SCNs can reflect brain structural architecture at a group level and this architecture can tolerate disease development albeit to different extents in the two groups. Specifically, HIG displayed a lower Sigma, suggestive of a more compromised trade-off between information processing and wiring costs relative to LIG. Moreover, the higher C_p in HIG indicates a higher prevalence of local cliquishness (a more segregated network), which may result from the enhanced intra-network (within somatomotor network) and inter-network connections (between somatomotor network and

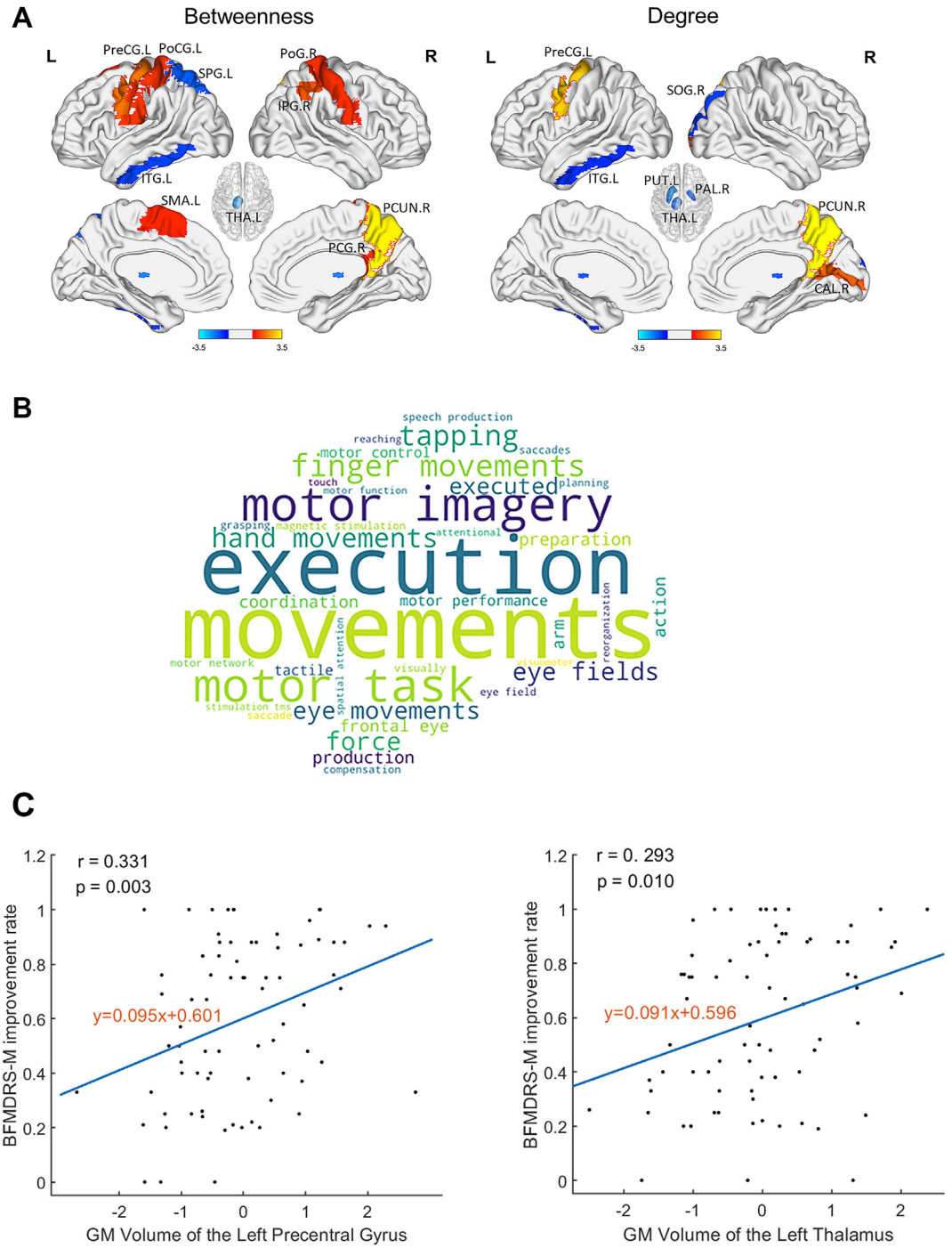

Fig. 3. Results of nodal network analyses, functional annotation, and correlation analyses. (A) Spatial distribution of the nodes showing discrepant betweennesses (left) and degrees (right) between HIG and LIG (permutation tests, $P < 0.05$, uncorrected). The discrepant regions are mapped onto the cortical surface (subcortical nuclei are rendered separately) and illustrated in warm color (HIG > LIG) or in cold color (HIG < LIG) using the BrainNet Viewer software (https://www.nitrc.org/projects/bnv/). The color bar represents the value of log(1/*P*). (B) Functional annotation of the brain regions showing between-group differences in betweenness or degree. The words in the figure represent the probable biological functions related to these brain regions. The font sizes of these words are scaled in terms of their correlation coefficients with the meta-analytic co-activation maps, which were provided by the Neurosynth database after we submitted the binary mask involving these differential brain regions to it. (C) Relationship between the BFMDRS-M improvement rates and the mean GM volume of regions showing differences in both betweenness and degree (Spearman correlation, $P < 0.0125$, Bonferroni corrected). The x-axis denotes the standardized residuals of the mean GM volume of these regions after regressing out the effects of sex, age, total intracranial volume, and education.

DMN) in HIG revealed by the interregional connectivity analyses. The E_{global} and L_p are reciprocal, both denoting the information transfer efficiency through the whole brain. The longer L_p and the lower E_{global} in HIG indicate an impairment of network integration, which may be caused by the loss of long-distance connections. Together, all the above alterations denote that the SCN constructed in HIG developed towards a regular network organization — manifesting as higher fault tolerance (higher C_p) but lower ability of global information transfer (higher L_p)

Table 2
Regions showing discrepant nodal centralities between HIG and LIG (AAL2 Atlas).

Abbreviation	Brain Regions	*P* value	
		Betweenness	Degree
HIG > LIG			
PreCG.L	Left precentral gyrus	**0.007**	**0.001***
SMA.L	Left supplementary motor area	**0.041**	0.121
PCG.R	Right posterior cingulate gyrus	**0.036**	0.177
CAL.R	Right calcarine fissure and surrounding cortex	0.141	**0.011**
PoCG.L	Left postcentral gyrus	**0.028**	0.154
PoCG.R	Right postcentral gyrus	**0.034**	0.121
IPG.R	Right inferior parietal gyrus - excluding supramarginal and angular gyri	**0.011**	0.131
PCUN.R	Right precuneus	**0.0004***	**0.0002***
HIG < LIG			
SOG.R	Right superior occipital gyrus	0.186	**0.022**
SPG.L	Left superior parietal gyrus	**0.046**	0.131
PUT.L	Left putamen	0.249	**0.009**
PAL.R	Right pallidum	0.306	**0.012**
THA.L	Left thalamus	**0.004**	**0.012**
ITG.L	Left inferior temporal gyrus	**0.021**	**0.033**

P values are computed by non-parametric permutation tests. Significant *P* values (two-tailed, $P < 0.05$, uncorrected) are shown in bold. Results corrected for multiple comparisons are indicated with an asterisk ($P < 0.05$, Benjamini-Hochberg FDR correction). HIG, high-improvement group; LIG, low-improvement group.

(see Fig S1). Since DBS works by normalizing the disrupted brain network [43], we may interpret these findings as the HIG presenting higher improvement in motor symptoms by leaving more room for STN-DBS to correct the disrupted network. Moreover, the preoperative BFMDRS-M scores displayed no difference between groups (Table 1), which indicated that the degree of large-scale SCN change was independent of the symptomatic severity.

Interpretation of the differences in nodal network measures

Between-group comparisons of nodal network topologies revealed several regions showing potential relevance to STN-DBS outcomes, and functional annotation indicated that these regions were associated with the function of movement. This indicated that the topological properties of the motor-related brain regions were associated with STN-DBS outcomes, which was consistent with how STN-DBS works, i.e., correcting the dysfunctional sensorimotor networks. Moreover, the correlation analyses identified the relationship between symptomatic improvement rates and the GM volume of the left precentral gyrus and left thalamus, suggesting that the discrepancies in nodal centralities were probably related to the differences in regional volume.

Among the brain regions showing discrepant nodal centralities, the precuneus consistently survived the multiple comparison corrections in the comparisons of nodal centralities, hinting at its dominant role in

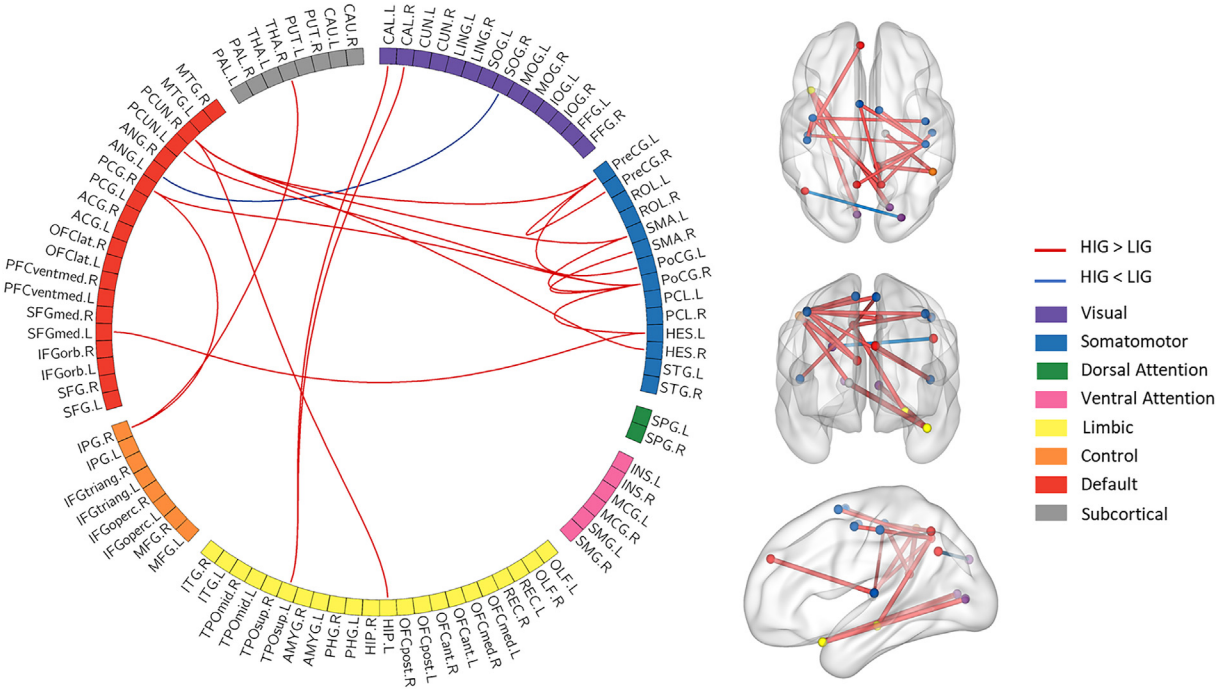

Fig. 4. Circular and anatomical distribution of the results of interregional connectivity analyses. Ninety-four cerebral regions of AAL2 (no cerebellum) are mapped to the Yeo seven networks with the subcortical nuclei labeled as the eighth network. The significantly altered edges (permutation tests, $P < 0.001$, uncorrected) are displayed in red (HIG > LIG) or in blue (HIG < LIG). The circular distribution (left) of the different edges is displayed by using the Circos software (https://www.circos.ca/software). The anatomical distribution (right) of the different edges is exhibited by using the BrainNet Viewer software (https://www.nitrc.org/projects/bnv/) with each region located according to their centroid stereotaxic coordinates and the thickness of each edge representing the degree of between-group difference (log(1/*P*)). See Table S2 for annotation of brain region abbreviations.

differentiating HIG from LIG. The structural alteration of precuneus had been identified by a previous comparison between MS and HC [44], and its GM volume showed a difference between the moderate-DBS-outcome group and the superior-DBS-outcome group [13]. Another functional study about laryngeal dystonia patients also found that the activity in the left precuneus was associated with the short-term outcome of botulinum injection [45]. Recent tractography studies found that the precuneus is a heterogeneous region that has widespread white matter connections with other brain structures, including those showing differential betweennesses or degrees in this article, such as the parietal lobes, supplementary motor area, lateral occipital cortex, and temporal lobe [46,47]. Also, the precuneus has been deemed as a highly functional region, not only participating in the visuospatial processing and sensory integration, but also playing a critical role in complex cognitive tasks, such as episodic and working memory, theory of mind, self-referential thinking, and sensorimotor dynamics [48]. The decreased nodal centralities in the precuneus in LIG indicate its compromised role in coordinating multiple brain regions and integrating multiple functions, which may further interfere with the efficacy of STN-DBS.

The disorganization of the somatomotor network (including basal ganglia, thalamus, sensorimotor cortex, and cerebellum) has been thought to be the main pathogenesis of MS by plenty of previous studies [15,17–19,49]. In this study, we further detected different nodal centralities in the sensorimotor cortex and subcortical nuclei between groups, and the GM volume of the left precentral gyrus and left thalamus was positively correlated with the BMFDRS-M scores. Further interregional connectivity analyses also revealed altered connections involving the sensorimotor cortex. All these results suggest that the sensorimotor cortex and subcortical nuclei (especially the left precentral gyrus and the left thalamus) are not only related to MS progression but also associated with STN-DBS outcomes. Since STN has extensive fiber connections with the thalamus and sensorimotor cortex [50], it is not difficult to understand that the structural alterations of these brain regions would influence the efficacy of STN-DBS. Although no previous study about MS has correlated the DBS outcomes with the structural and functional alterations of the sensorimotor cortex and subcortical nuclei, a GPi-DBS study about generalized dystonia indicated that structural and functional connectivity between the bilateral GPi and the primary sensorimotor cortex was correlated with symptomatic improvement [51]. Another structural MRI study about generalized and cervical dystonia found that a better chronic GPi-DBS outcome was associated with hypertrophy of the supplementary motor area [14]. Furthermore, the effect of the sensorimotor areas on DBS efficacy can also be mirrored by the studies on Parkinson's disease because of the same stimulation targets. For example, a higher STN-DBS efficacy was correlated with a thicker precentral cortex in Parkinson's disease [52]. In addition, in this study, we found that the betweenness and degree tended to increase in the sensorimotor cortex but decrease in subcortical nuclei in HIG. The changing directions cater to the possible mechanism of STN-DBS revealed by DBS-ON functional MRI studies, that is, STN-DBS induced activation of the GPi and thalamus but deactivation of the precentral gyrus [12,53]. This may partly explain why HIG possessed a better STN-DBS responsiveness.

In addition, the significant differences in nodal centralities of most brain regions showed a unilateral pattern (Table 2). We think that the hemispherical laterality in nodal centralities is due to several factors. First, hemispherical laterality exists in normal motor control (e.g., most people are right-handed). This laterality in motor control can be amplified in DBS responders (HIG), though the handedness showed no difference between HIG and LIG (Table 1). Second, the relatively small number of subjects in each group may have reduced the sensitivity to detecting symmetry changes. As shown in Fig. S4, the nodal centralities of the contralateral nodes changed in almost the same direction as the nodes with significant between-group differences (i.e., synchronized increases or decreases), but just not yet to the level of statistical testing. We speculate that large-sample studies will improve the detection rate of symmetrical changes in the future. Finally, we detected laterality at the group level, but this does not mean that all individuals must exhibit laterality in the same direction. Future individual SCN analysis will directly assess the asymmetry in each subject.

Interpretation of the validation results

In this study, we used the HOA to validate the results of the AAL2 atlas and obtained similar results, which further verified the reliability and reproducibility of SCN-based graph theory analyses. Even so, there still exist certain atlas-related differences. For example, for the between-group comparisons of the global topological properties, the E_{global} showed a significant difference in the AAL2 results but no difference in the HOA results. And the comparisons of nodal topological properties yielded some non-overlapping brain regions. We speculate that these inconsistencies come from the different node numbers of the two atlases and the different cortical parcellation schemes. Previous studies have shown that differences in network size (i.e., number of nodes) can significantly affect the topological properties of functional and structural brain networks [54,55]. Moreover, different cortical parcellation schemes generated different brain region sizes, which can affect the measurement of the mean GM volume of each ROI, leading to differences in pairwise interregional Pearson correlations (SCNs). This relationship between regional size and nodal centrality has also been unearthed by previous functional and morphological brain network studies [54–56].

Limitations

Our study carries the following limitations. First, considering the importance of the subcortical nuclei, we only explored volume-based differences between the two groups. Whether surface-based analyses could yield analogous results needs to be investigated in the future. Second, we only performed comparisons of SCN-based graph theory metrics. Currently, we still lack a clear understanding of the cellular and molecular mechanisms underlying SCNs. To what extent the SCN-based results are consistent with diffusional or functional results still needs to be explored further. Third, there still existed certain non-overlapping topological changes between the two atlases used in this study. Fourth, the results of this study are based on single-center data, and whether these significant findings stably exist in other independent datasets still needs further validation. Finally, compared with diffusional and functional networks, the group-level SCNs cannot generate individual metrics, thereby limiting the exploration of relationships between network metrics and clinical variables, and the prediction of DBS outcomes using network metrics.

In summary, good and poor STN-DBS responders have discrepant large-scale topological properties of SCNs with good responders showing a trend towards a regular network. STN-DBS outcomes are predominantly associated with the topological and volumetric changes in the precuneus, sensorimotor cortex, and subcortical nuclei. These findings extend our understanding of the neuroimaging mechanisms related to STN-DBS outcomes from a network perspective.

Funding

This work was funded by the National Natural Science Foundation of China, China (No. 81871087 and No. 82001798), the STI, China 2030 – Major Projects (2021ZD0200407), and the Young Talent Project of Chinese PLA General Hospital, China (No. 20230403).

Author contributions

Study design: ZYY and YXG; Study execution: LB and MZQ; Statistical analysis: LB and YH; Drafting the manuscript: LB; Revision of manuscript: YXY, XJP, LB, and FZB; Study coordination: YXG.

Declaration of competing interest

The authors declare that they have no known competing financial interests or personal relationships that could have appeared to influence the work reported in this paper.

Acknowledgments

We want to thank all the patients for their participation.

Appendix A. Supplementary data

Supplementary data to this article can be found online at https://doi.org/10.1016/j.neurot.2024.e00367.

References

[1] Pandey S, Sharma S. Meige's syndrome: history, epidemiology, clinical features, pathogenesis and treatment. J Neurol Sci 2017;372:162–70.
[2] Wang X, Zhang Z, Mao Z, Yu X. Deep brain stimulation for Meige syndrome: a meta-analysis with individual patient data. J Neurol 2019;266(11):2646–56.
[3] Zheng W, Lv G, Lu Y, Liu J, Hao Q, Ding H, et al. Bilateral pallidal deep brain stimulation in meige syndrome: effects on motor function, neuropsychological status, and mood. Neurosurgery 2023;92(5):1073–9.
[4] Reese R, Gruber D, Schoenecker T, Bazner H, Blahak C, Capelle HH, et al. Long-term clinical outcome in meige syndrome treated with internal pallidum deep brain stimulation. Mov Disord 2011;26(4):691–8.
[5] Zhan S, Sun F, Pan Y, Liu W, Huang P, Cao C, et al. Bilateral deep brain stimulation of the subthalamic nucleus in primary Meige syndrome. J Neurosurg 2018;128(3):897–902.
[6] Wang X, Mao Z, Cui Z, Xu X, Pan L, Liang S, et al. Predictive factors for long-term clinical outcomes of deep brain stimulation in the treatment of primary Meige syndrome. J Neurosurg 2019;132(5):1367–75.
[7] Ouyang J, Hao Q, Zhu R, Wu G, Ding H, Wang D, et al. Subthalamic nucleus deep brain stimulation in primary meige syndrome: a 1-year follow-up study. Neuromodulation 2021;24(2):293–9.
[8] Tisch S. Deep brain stimulation in dystonia: factors contributing to variability in outcome in short and long term follow-up. Curr Opin Neurol 2022;35(4):510–7.
[9] Yao C, Horn A, Li N, Lu Y, Fu Z, Wang N, et al. Post-operative electrode location and clinical efficacy of subthalamic nucleus deep brain stimulation in Meige syndrome. Parkinsonism Relat Disorders 2019;58:40–5.
[10] Isaias IU, Volkmann J, Kupsch A, Burgunder JM, Ostrem JL, Alterman RL, et al. Factors predicting protracted improvement after pallidal DBS for primary dystonia: the role of age and disease duration. J Neurol 2011;258(8):1469–76.
[11] Liu B, Mao Z, Cui Z, Ling Z, Xu X, He K, et al. Cerebellar gray matter alterations predict deep brain stimulation outcomes in Meige syndrome. Neuroimage Clin 2023;37:103316.
[12] Loh A, Elias GJB, Germann J, Boutet A, Gwun D, Yamamoto K, et al. Neural correlates of optimal deep brain stimulation for cervical dystonia. Ann Neurol 2022;92(3):418–24.
[13] Wu Y, Zhang C, Li Y, Feng J, Zhang M, Li H, et al. Imaging insights of isolated idiopathic dystonia: voxel-based morphometry and activation likelihood estimation studies. Front Neurol 2022;13:823882.
[14] Fecikova A, Jech R, Cejka V, Capek V, Stastna D, Stetkarova I, et al. Benefits of pallidal stimulation in dystonia are linked to cerebellar volume and cortical inhibition. Sci Rep 2018;8(1):17218.
[15] Zheng Z, Pan P, Wang W, Shang H. Neural network of primary focal dystonia by an anatomic likelihood estimation meta-analysis of gray matter abnormalities. J Neurol Sci 2012;316(1-2):51–5.
[16] Chirumamilla VC, Dresel C, Koirala N, Gonzalez-Escamilla G, Deuschl G, Zeuner KE, et al. Structural brain network fingerprints of focal dystonia. Ther Adv Neurol Disord 2019;12:1756286419880664.
[17] Battistella G, Termsarasab P, Ramdhani RA, Fuertinger S, Simonyan K. Isolated focal dystonia as a disorder of large-scale functional networks. Cerebr Cortex 2017;27(2):1203–15.
[18] Cheng Q, Xiao H, Luo Y, Zhong L, Guo Y, Fan X, et al. Cortico-basal ganglia networks dysfunction associated with disease severity in patients with idiopathic blepharospasm. Front Neurosci 2023;17:1159883.
[19] Guo Y, Peng K, Liu Y, Zhong L, Dang C, Yan Z, et al. Topological alterations in white matter structural networks in blepharospasm. Mov Disord 2021;36(12):2802–10.
[20] He Y, Chen Z, Evans A. Structural insights into aberrant topological patterns of large-scale cortical networks in Alzheimer's disease. J Neurosci 2008;28(18):4756–66.
[21] Evans AC. Networks of anatomical covariance. Neuroimage 2013;80:489–504.
[22] Alexander-Bloch A, Giedd JN, Bullmore E. Imaging structural co-variance between human brain regions. Nat Rev Neurosci 2013;14(5):322–36.
[23] Alexander-Bloch A, Raznahan A, Bullmore E, Giedd J. The convergence of maturational change and structural covariance in human cortical networks. J Neurosci 2013;33(7):2889–99.
[24] Kelly C, Toro R, Di Martino A, Cox CL, Bellec P, Castellanos FX, et al. A convergent functional architecture of the insula emerges across imaging modalities. Neuroimage 2012;61(4):1129–42.
[25] Lerch JP, Worsley K, Shaw WP, Greenstein DK, Lenroot RK, Giedd J, et al. Mapping anatomical correlations across cerebral cortex (MACACC) using cortical thickness from MRI. Neuroimage 2006;31(3):993–1003.
[26] Gong G, He Y, Chen ZJ, Evans AC. Convergence and divergence of thickness correlations with diffusion connections across the human cerebral cortex. Neuroimage 2012;59(2):1239–48.
[27] Romero-Garcia R, Whitaker KJ, Vasa F, Seidlitz J, Shinn M, Fonagy P, et al. Structural covariance networks are coupled to expression of genes enriched in supragranular layers of the human cortex. Neuroimage 2018;171:256–67.
[28] Sporns O. Structure and function of complex brain networks. Dialogues Clin Neurosci 2013;15(3):247–62.
[29] Fornito A, Zalesky A, Breakspear M. Graph analysis of the human connectome: promise, progress, and pitfalls. Neuroimage 2013;80:426–44.
[30] Burke RE, Fahn S, Marsden CD, Bressman SB, Moskowitz C, Friedman J. Validity and reliability of a rating scale for the primary torsion dystonias. Neurology 1985;35(1):73–7.
[31] Rolls ET, Joliot M, Tzourio-Mazoyer N. Implementation of a new parcellation of the orbitofrontal cortex in the automated anatomical labeling atlas. Neuroimage 2015;122:1–5.
[32] Yeo BT, Krienen FM, Sepulcre J, Sabuncu MR, Lashkari D, Hollinshead M, et al. The organization of the human cerebral cortex estimated by intrinsic functional connectivity. J Neurophysiol 2011;106(3):1125–65.
[33] Buckner RL, Krienen FM, Castellanos A, Diaz JC, Yeo BT. The organization of the human cerebellum estimated by intrinsic functional connectivity. J Neurophysiol 2011;106(5):2322–45.
[34] Zhang J, Wang J, Wu Q, Kuang W, Huang X, He Y, et al. Disrupted brain connectivity networks in drug-naive, first-episode major depressive disorder. Biol Psychiatr 2011;70(4):334–42.
[35] Watts DJ, Strogatz SH. Collective dynamics of 'small-world' networks. Nature 1998;393(6684):440–2.
[36] Hosseini SM, Black JM, Soriano T, Bugescu N, Martinez R, Raman MM, et al. Topological properties of large-scale structural brain networks in children with familial risk for reading difficulties. Neuroimage 2013;71:260–74.
[37] Rubinov M, Sporns O. Complex network measures of brain connectivity: uses and interpretations. Neuroimage 2010;52(3):1059–69.
[38] Yarkoni T, Poldrack RA, Nichols TE, Van Essen DC, Wager TD. Large-scale automated synthesis of human functional neuroimaging data. Nat Methods 2011;8(8):665–70.
[39] Wang Z, Shu H, Liu D, Su F, Xie C, Cui Z, et al. Predictions of current and future episodic memory using grey matter volume and functional connectome: a longitudinal study in amnestic mild cognitive impairment patients. Research Square [Preprint] 2020 Jun 3. Available from: https://doi.org/10.21203/rs.3.rs-31020/v2.
[40] Desikan RS, Segonne F, Fischl B, Quinn BT, Dickerson BC, Blacker D, et al. An automated labeling system for subdividing the human cerebral cortex on MRI scans into gyral based regions of interest. Neuroimage 2006;31(3):968–80.
[41] Xue A, Kong R, Yang Q, Eldaief MC, Angeli PA, DiNicola LM, et al. The detailed organization of the human cerebellum estimated by intrinsic functional connectivity within the individual. J Neurophysiol 2021;125(2):358–84.
[42] King M, Hernandez-Castillo CR, Poldrack RA, Ivry RB, Diedrichsen J. Functional boundaries in the human cerebellum revealed by a multi-domain task battery. Nat Neurosci 2019;22(8):1371–8.
[43] Aum DJ, Tierney TS. Deep brain stimulation: foundations and future trends. Front Biosci (Landmark Ed). 2018;23(1):162–82.
[44] Liu J, Li L, Chen L, Liu R, Jiang Y, Fang J, et al. Grey matter changes in Meige syndrome: a voxel-based morphology analysis. Sci Rep 2020;10(1):14533.
[45] O'Flynn LC, Simonyan K. Short- and long-term central action of botulinum neurotoxin treatment in laryngeal dystonia. Neurology 2022;99(11):e1178–90.
[46] Tanglay O, Young IM, Dadario NB, Briggs RG, Fonseka RD, Dhanaraj V, et al. Anatomy and white-matter connections of the precuneus. Brain Imaging Behav 2022;16(2):574–86.
[47] Jitsuishi T, Yamaguchi A. Posterior precuneus is highly connected to medial temporal lobe revealed by tractography and white matter dissection. Neuroscience 2021;466:173–85.
[48] Dadario NB, Sughrue ME. The functional role of the precuneus. Brain 2023;146(9):3598–607.
[49] Mascia MM, Dagostino S, Defazio G. Does the network model fits neurophysiological abnormalities in blepharospasm? Neurol Sci 2020;41(8):2067–79.
[50] Quartarone A, Cacciola A, Milardi D, Ghilardi MF, Calamuneri A, Chillemi G, et al. New insights into cortico-basal-cerebellar connectome: clinical and physiological considerations. Brain 2020;143(2):396–406.
[51] Okromelidze L, Tsuboi T, Eisinger RS, Burns MR, Charbel M, Rana M, et al. Functional and structural connectivity patterns associated with clinical outcomes in deep brain stimulation of the globus pallidus internus for generalized dystonia. AJNR Am J Neuroradiol 2020;41(3):508–14.
[52] Chen Y, Zhu G, Liu Y, Liu D, Yuan T, Zhang X, et al. Predict initial subthalamic nucleus stimulation outcome in Parkinson's disease with brain morphology. CNS Neurosci Ther 2022;28(5):667–76.
[53] Shen L, Jiang C, Hubbard CS, Ren J, He C, Wang D, et al. Subthalamic nucleus deep brain stimulation modulates 2 distinct neurocircuits. Ann Neurol 2020;88(6):1178–93.

[54] Wang J, Wang L, Zang Y, Yang H, Tang H, Gong Q, et al. Parcellation-dependent small-world brain functional networks: a resting-state fMRI study. Hum Brain Mapp 2009;30(5):1511–23.
[55] Li Y, Wang N, Wang H, Lv Y, Zou Q, Wang J. Surface-based single-subject morphological brain networks: effects of morphological index, brain parcellation and similarity measure, sample size-varying stability and test-retest reliability. Neuroimage 2021;235:118018.
[56] Seidlitz J, Vasa F, Shinn M, Romero-Garcia R, Whitaker KJ, Vertes PE, et al. Morphometric similarity networks detect microscale cortical organization and predict inter-individual cognitive variation. Neuron 2018;97(1):231–247 e7.